UDC 544.47:544.344
https://doi.org/10.15407/kataliz2020.29.001

Efficient hydrogen production by steam reforming of ethanol over ferrite catalysts

L.Yu. Dolgikh, I.L. Stolyarchuk, L.A. Staraya, I.V. Vasylenko, Y.I. Pyatnitsky, P.E. Strizhak

L.V. Pisarzhevsky Institute of Physical Chemistry, National Academy of Sciences of Ukraine, Prospekt Nauky, 31, Kyiv 03028, Ukraine. E-mail: yupyat@gmail.com

Steam reforming of ethanol is considered nowadays to be attractive mode of production of hydrogen as the most viable energy carrier for the future. Additionally, producing hydrogen from ethanol steam reforming would be environmentally friendly. Ethanol can be prepared from agricultural residues and hence is a renewable resource. Its producing from biomass fermentation is enough simple and cheap way. Besides operating conditions, the use of catalysts plays a crucial role in hydrogen production through ethanol reforming. Different catalysts have been used for the steam reforming of ethanol, in the great majority of cases, supported noble metals, nickel and cobalt. The present work is devoted to investigation of the ethanol steam reforming over ferrites as novel oxide type of catalysts for this reaction. The ferrite catalysts, MFe_2O_4 (M = Mg, Mn, Fe, Zn), have been prepared by coprecipitation method; to characterize the catalysts, the methods of X-ray diffraction, electron diffraction, BET, temperature programmed desorption of CO_2, the thermal gravimetry have been used. The catalytic experiments have been performed at atmospheric pressure in the temperature range 573-823°K. The main reaction products were acetaldehyde, acetone, CO_2 and H_2. It is important to note, that CO, which is undesirable impurity in hydrogen, was not appeared in the reaction products. At relatively low temperatures, high selectivity for acetone (71.3 %), that is very close to its theoretical value (75 %), was observed for $FeFe_2O_4$. Thus, the $FeFe_2O_4$ ferrite can be considered as an efficient catalyst for the direct conversion of ethanol to acetone. At higher temperatures, selectivity to acetone decreases due to acetone conversion to CO_2 and the target product H_2. The selectivity to hydrogen increases up to 823 K for all investigated ferrites. Maximum hydrogen yield (83.4 %) was achieved for $MnFe_2O_4$, therefore it is a promising object for further study.

Key words: ethanol, steam reforming, ferrite catalysts, hydrogen

Introduction

The ethanol steam reforming (ESR) is an attractive, sustainable and environment friendly route for production of hydrogen as extremely clean energy source with relatively high energy conversion and low air pollution. The ethanol produced renewably by fermentation of different biomass sources is called bioethanol, which is a mixture of ethanol and water with molar ratio about 1:13 [1]. Currently, there are three generations of bioethanol, based on different feedstocks [2]. The first generation of bioethanol is produced by fermentation of glucose obtained from sugar crops (sugarcane and sugar beet) and starch crops (wheat, barley, corn and potato). Second generation bioethanol production uses lignocellulosic resources and agricultural residues as starting materials (straw, wood, herbaceous biomass, cellulose waste). Third-generation bioethanol can be produced from marine organisms such as seaweeds. The advantage of the second and third generations is their limited competition with human food.

The research interest in the area of catalytic ESR reaction has been increased in the last 2 decades as evidences by reviews [3-10]. Most studies have been performed over supported noble metals (Pt, Pd, Rh, Ru, Ir) [11-20], Ni [21-25], and Co [26-30]. Recently, spinel-type oxides [31, 32] and perovskites [33-35] have been employed as catalysts for ESR reaction. The spinel-type oxide $NiAl_2O_4$ showed extremely stable performance for 48 h at 823 K (the ethanol conversion was almost 100%, the CO_2, CO and CH_4 selectivity were around 80%, 10% and 10 %, respectively), whereas activity of $NiFe_2O_4$ and $NiMn_2O_4$ was continuously reduced in time [31]. According to XRD data, $NiMn_2O_4$ was completely destroyed to Ni and MnO after catalysis; $NiFe_2O_4$ was partially destroyed with a formation of Ni and Fe_3O_4, whereas the crystalline structure of $NiAl_2O_4$ remained practically unchanged. Nevertheless, it was supposed that catalytic action of all these catalysts is determined by metallic Ni which is generated under reaction conditions [31].

Another type of complex oxides, perovskites La_2NiO_4, $LaFe_yNi_{1-y}O_3$ and $LaCo_{1-x}Zn_xO_3$, was also found to be catalytically active in the ESR reaction [33-35]. It was shown that structure of La_2NiO_4 was destroyed to Ni-La_2O_3 during catalysis. However, the obtained composition showed fairly good catalytic performance at 923 K [33]. The catalytic activity of perovskite-type oxide $LaFe_yNi_{1-y}O_3$ was significantly higher than activity of the supported catalyst

$NiO/LaFeO_3$ with the same gross composition [34]. $LaCo_{0.9}Zn_{0.1}O_3$ perovskite shown high stability in the conditions of the ESR reaction and demonstrates hydrogen selectivity about 80 % [35]. High hydrogen yield in the ESR reaction over spinel $MnFe_2O_4$ was achieved in our previous work [36].

All these studies indicate that spinel and perovskite type oxides may be considered as promising catalysts for the ESR reaction. The aim of this work is to study a catalytic performance of the novel catalysts for the ESR reaction: spinel-type ferrites $M^{II}Fe_2O_4$ (M = Mg, Mn, Zn, Fe).

Experimental

Catalyst preparation

The manganese ferrite $MnFe_2O_4$ was prepared by a chemical co-precipitation method. NH_3 water solution was dropped to a water solution of Fe(III) and Mn(II) nitrates with molar ratio 2:1 under vigorous stirring, then the produced brown reaction mixture was cured at 363 K during 5 h with continuous stirring. The obtained precipitate was separated by magnetic decantation, washed with water, ethanol and diethyl ether, dried at room temperature and calcinated at 673 K for 2 h. Commercially available chemically-pure grade and analytical grade reagents were used without additional purification.

Ferrites MFe_2O_4 (M = Mg, Fe, Zn) were synthesized by similar procedure [37-39]. The aqueous solutions of Fe(III) and M(II) nitrates were used (chlorides for M = Fe). Finally, the prepared samples were calcinated at 673 K for 2 h (in nitrogen flow for M = Fe to avoid oxidation of Fe(II)).

Catalyst characterization

X-Ray diffraction measurements (XRD) were carried out with a Bruker D8 Advance diffractometer, with a Cu-anode, $\lambda = 0.154$ nm, step $2\theta = 0.050$, exposition time 5 s/step. Identification of crystalline phases was performed by matching with the ICDD files in the PDF-2 Version 2.0602 (2006) database. BET surface areas were measured by using a Sorptomatic 1990 instrument by adsorption of nitrogen at 77 K. Electron diffraction analysis (EDA) was conducted on a PEM-125K transmission electron microscope (Selmi, Ukraine) with accelerating voltage 100 kV.

In order to evaluate the basicity of the oxide surface, CO_2-TPD experiments were carried out with a conventional setup equipped with a TCD detector. The catalyst samples were first purged with He at 623 K for 2 h, then cooled down to room temperature. The adsorption of CO_2 was carried out using a feed mixture of 50 vol.% CO_2/He for 30 min. The reactor was then purged with He for 2 h. After that the temperature was increased to 823 K with a heating rate of 10 K/min under He flow (40 ml/min). The change in thermal conductivity is due to the concentration change of CO_2 in the effluent was recorded. The CO_2-TPD signals were referred to 1 m^2 of surface area of the samples.

Hydrogen temperature-programmed reduction (H_2-TPR) was performed with the same setup. A catalyst sample was pretreated at 523 K for 2 h under flowing Ar (50 ml/min). After cooling to room temperature, the sample was exposed to a flow of 10 vol.% H_2/He (50 ml/min), and the temperature was increased linearly at 10 K/min.

To elucidate the influence of catalyst calcinations on a catalyst state, the thermal gravimetric method was performed. The curves of mass loss (TG) as well as of differential thermal analysis (DTA) and differential gravimetric analysis (DTG) were registered with a thermal gravimetric analysis system Q-1500 (supplied by MOM instruments, Budapest) with an air flow from 298 to 1273 K at a heating rate of 10 K/min; a sample mass was of 0.4 to 0.6 g.

Catalytic tests

The ESR reaction was carried out in a fixed-bed tubular quartz reactor at atmospheric pressure with the temperature increased stepwise from 573 to 823 K at molar ratio $H_2O/C_2H_5OH=19$ (2.7 mol.% C_2H_5OH, 50 vol.% H_2O, N_2 balance) that is close to water/ethanol relation in bioethanol obtained by fermentation. The procedure of catalytic tests and reaction mixture analysis were as described elsewhere [40]. A catalyst, approx. 1 g, of particle size between 1 and 2 mm, was placed in a reactor between two layers of quartz grains of the same diameter; it was held at each temperature for 1 h, followed by gas chromatography analysis. At the end of a catalytic test at 823 K, the flow of reaction mixture was stopped and a catalyst was cooled under N_2 stream and stored for characterization.

Ethanol conversion, X, and selectivity of carbon-based reaction products, S_{Cn}, were evaluated according to the following expressions:

$$X = \frac{\sum n \cdot F_{Cn}}{2 \cdot F_{Et,in}} \cdot 100 \quad (1)$$

$$S_{Cn} = \frac{n \cdot F_{Cn}}{\sum n \cdot F_{Cn}} \cdot 100 \quad (2)$$

where n is a number of C-atoms in a product C_n; $F_{Et,in}$ is an inlet feed of ethanol, mol h^{-1}; F_{Cn} is a feed of corresponding product, mol h^{-1}.

The selectivity of hydrogen was defined as 100%, when 6 mol of H_2 were formed per 1 mol of reacted C_2H_5OH. Then:

$$S_{H2} = \frac{F_{H2}}{3 \cdot \sum n \cdot F_{Cn}} \cdot 100 \quad (3)$$

where F_{H2} is an outlet feed of hydrogen, mol h^{-1}.

Hydrogen yield, Y_{H2}, was calculated as:

$$Y_{H2} = X \cdot S_{H2} \quad (4)$$

Results and Discussion

Catalyst stability

According to X-ray diffraction data, reflexes in XRD patterns of the fresh samples of $FeFe_2O_4$, $MnFe_2O_4$, $MgFe_2O_4$ ferrites calcined at 673 K were not observed ($ZnFe_2O_4$ was poorly crystallized). This can be explained by too small size of catalyst particles. Identification of the ferrite crystalline phases was made by electron diffraction analysis. For example, electron diffraction patterns of the $FeFe_2O_4$ sample are given in Fig.1.

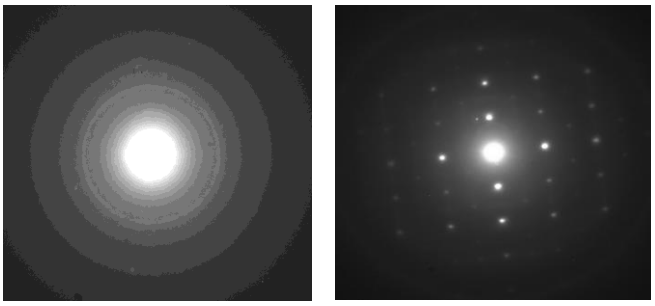

Fig.1. Electron diffraction patterns of $FeFe_2O_4$ before (left) and after (right) catalysis at 823 K

After increasing of calcinations temperature to 873 K in air manganese ferrite remained in amorphous state during 4 h, and while it was transformed to Mn_2O_3(ICDD N 01-089-2809) and Fe_2O_3(ICDD N 01-085-0599) after 10 h calcination at the same temperature due to ferrite oxidation. In contrary, after catalysis all ferrite samples possessed a clear crystalline image with a structure of cubic spinel as shown in Fig. 2 (for identification of ferrite crystalline phases, we used ICDD N 00-019-0629 for $FeFe_2O_4$, ICDD N 01-074-2403 for $MnFe_2O_4$, ICDD N 01-088-1942 for $MgFe_2O_4$ and ICDD N 00-022-1012 for $ZnFe_2O_4$).

Crystallization of ferrites in the catalytic conditions was accompanied with a significant decreasing of its specific surface area (Table 1). The effect of influence on the ferrite crystallization may be associated with alternating acts of reduction and oxidation of a catalyst during the ethanol steam reforming reaction; oxygen defects formed in a reduction step make more easy migration of ions in the catalyst lattice and thus promote catalyst crystallization in the reaction conditions. Indeed, the specific surface area of $MgFe_2O_4$ was decreased from 121 to only 115 m^2 g^{-1} after calcinations at 823 K in air, while it was observed dramatically strong falling down of the specific surface area to 14 m^2 g^{-1} when $MgFe_2O_4$ was explored as a catalyst of ESR reaction (Table 1).

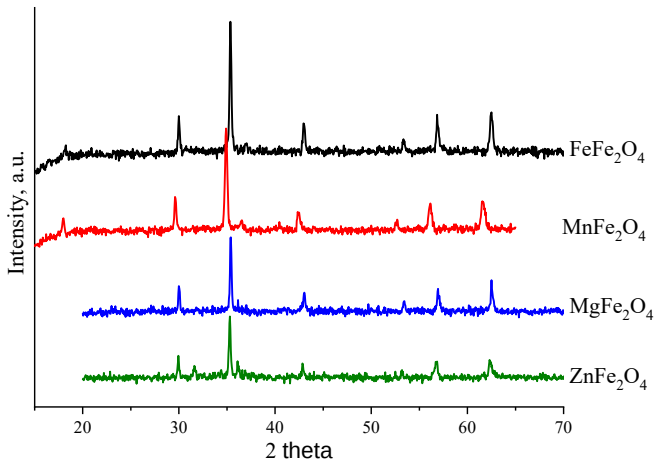

Fig. 2. XRD patterns of $FeFe_2O_4$, $MnFe_2O_4$, $MgFe_2O_4$ and $ZnFe_2O_4$ after catalysis at 823 K

Table 1. **Influence of the ESR reaction mixture (823 K, H_2O/C_2H_5OH = 19) on the catalyst specific surface area**

Catalyst	Specific surface area, m^2 g^{-1}	
	Before catalysis	After catalysis
$FeFe_2O_4$	220	18
$MnFe_2O_4$	140	10
$MgFe_2O_4$	121	14
$ZnFe_2O_4$	18	6

A thermal stability of the MFe_2O_4 (M = Fe, Mn, Zn, Mg) ferrites was also estimated by DTA-DTG method, obtained thermograms are presented in Fig.3. There are two temperature ranges of a mass loss. The first associated with water desorption was observed at 323-473 K with a maximum at 373-393 K; it was accompanied with an endothermic peak in the DTA curves. The mass loss at this temperature range was 11.6%, 12.7 %, 11.9% and 0.8% for $FeFe_2O_4$, $MnFe_2O_4$, $MgFe_2O_4$ and $ZnFe_2O_4$ respectively. The second temperature range of a mass loss was observed at 523-623 K for $FeFe_2O_4$ and at 573-673 K for $MgFe_2O_4$; it may be associated both with surface dehydroxylation as well as with decomposition of nitrate groups and organic compounds [41]. The mass loss was 5.7% for $FeFe_2O_4$ and 5.0% for $MgFe_2O_4$. Exothermal peaks at 553-593 K, that accompanied by mass loss for $FeFe_2O_4$, can be related to burning out of the organic solvent residues. The exothermic peaks at 803–853 K in DTA curves may be related to ferrospinel crystallization [42]. In these conditions, the cation migration from octahedral sites to tetrahedral ones may take place [42]. The total mass loss of the ferrite samples after their heating from 293 K to 1273 K was 21.2% for $FeFe_2O_4$; 15.8% for $MnFe_2O_4$; 20.3% for $MgFe_2O_4$ and 2.2% for $ZnFe_2O_4$.

Ferrite reducing ability

Catalyst reducing ability was estimated by the hydrogen temperature-programmed reduction method (H_2-TPR). The obtained results are shown in Fig.4.

The TPR profile of $FeFe_2O_4$ demonstrates complex structure. The peaks were separated using the Gaussian function and two overlapping peaks were recorded for the $FeFe_2O_4$ with maximum reduction temperatures 873 K and 966 K that may be attributed to reductive transformation $Fe^{3+} \rightarrow Fe^{2+}$ and $Fe^{2+} \rightarrow Fe^0$ respectively. The profile of $MnFe_2O_4$ consists of two peaks at 632 and 768 K. Peaks at 650 K and 719 K were found for TPR profile of $MgFe_2O_4$. It may be assumed that these peaks characterize the reduction of Fe^{3+} ions in octahedral (first peak) and tetrahedral (second peak) coordination. The reduction peak at 676 K was observed for $ZnFe_2O_4$ that may be associated with reduction $Fe^{3+} \rightarrow Fe^{2+,3+}$, while hydrogen consumption at T> 773 K may be a result of the reduction of Zn^{2+} to Zn^o, as well as $Fe^{2+,3+}$ to Fe^{2+}.

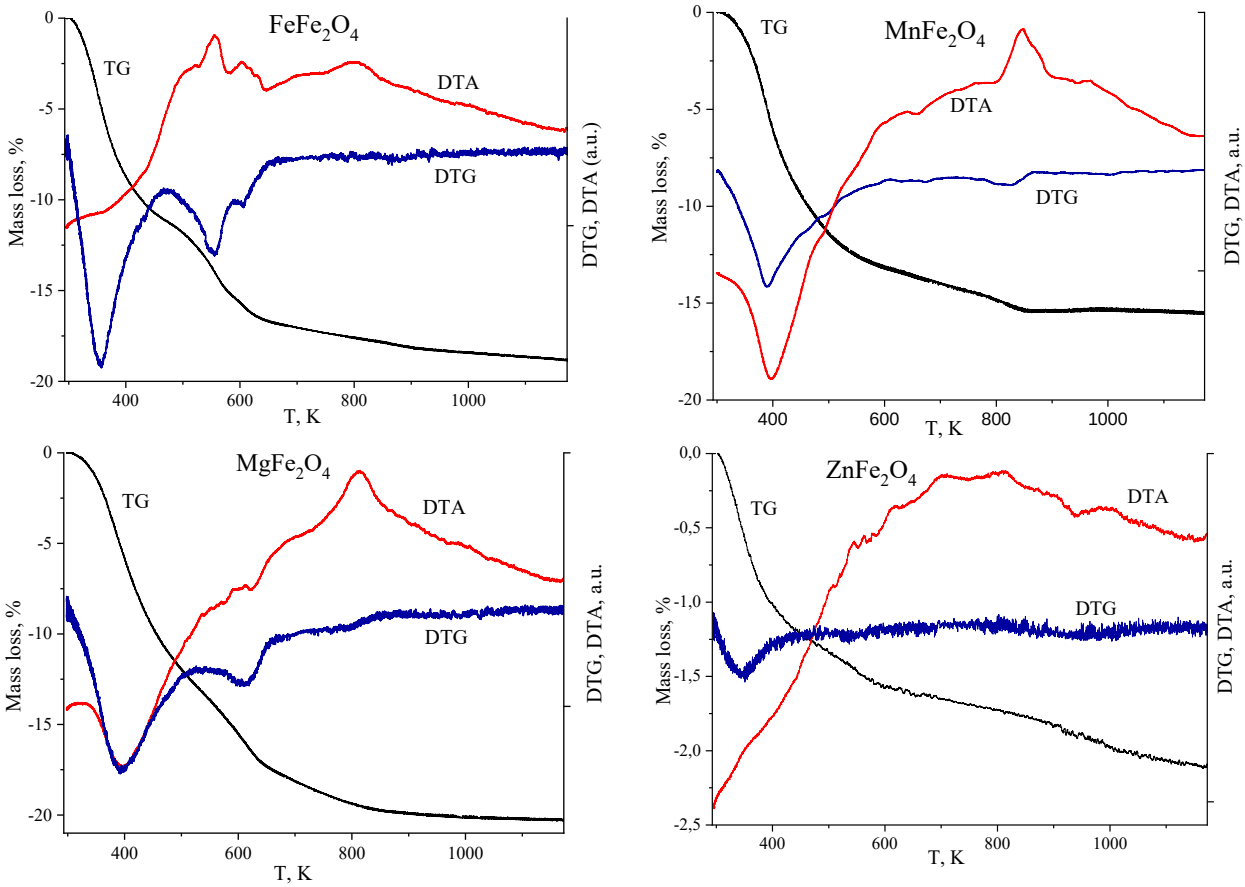

Fig.3. Thermograms of $FeFe_2O_4$, $MnFe_2O_4$, $MgFe_2O_4$ and $ZnFe_2O_4$

The TPR data highlight that the nature of metal M in the MFe_2O_4 ferrospinels influence significantly on the reductive ability of spinel Fe^{3+} ions. The order of reductive facility of Fe^{3+} to Fe^{2+} in spinels during $Fe_2O_3 \rightarrow Fe_3O_4$ transformation is as follows: $MnFe_2O_4 > MgFe_2O_4 > ZnFe_2O_4$.

Ferrite surface basicity

The rates of temperature programmed desorption of CO_2 normalized to surface area unit of the MFe_2O_4 (M = Fe, Mn, Mg, Zn) samples are presented in Fig.5.

The CO_2-TPD profiles of all ferrospinels are qualitatively similar in the range of 298-673 K; they can be divided to two peaks with maximum of 358-394 K (basic sites l) and 423-476 K (basic sites m). Basing on literature data [43-45], the low-temperature CO_2 desorption (about 373 K) may be related to the bicarbonate species which formed by CO adsorption on a weak basic OH group, the medium temperature desorption (about 473 K) may be related to bidentate carbonate species which formed due to CO_2 interaction with basic M-O pairs on the ferrite surface; they characterized as a medium strength basic sites.

Table 2 summarizes the CO_2-TPD measurements of the ferrite samples: temperature maxima of CO_2 desorption from low-temperature sites l (T_l) and from middle-temperature sites m (T_m); relative amounts of sites l (A_l) and sites m (A_m) as well as total amounts of basic sites per gram. The strength of sites m characterized by T_m changes in the order $MgFe_2O_4 > MnFe_2O_4 > FeFe_2O_4 > ZnFe_2O_4$. In addition, $MgFe_2O_4$ has the highest CO_2 uptake per gram. The relative amounts of l and m sites is approximately equal for $FeFe_2O_4$, l site amounts are higher than m site ones for $MnFe_2O_4$ and $MgFe_2O_4$ while only l sites were found out for $ZnFe_2O_4$.

As known, $FeFe_2O_4$, $MnFe_2O_4$ and $MgFe_2O_4$ have inverse spinel structures, while $ZnFe_2O_4$ has a normal spinel structure. Fe^{3+} ions in a normal spinel structure occupy octahedral sites which dominate on the surface of metal oxides with spinel structure [46]. Thus, it may be supposed that weak basic sites of $ZnFe_2O_4$ are OH-groups bonded to Fe^{3+} ions and a contribution of Zn-O pairs to $ZnFe_2O_4$ is negligible. In the case of inverse spinels such as $FeFe_2O_4$, $MnFe_2O_4$ and $MgFe_2O_4$, the metal bivalent ions M^{2+} replace trivalent ions in octahedral sites, thus it may influence both acid-basic and catalytic properties. The weak basic sites (l sites) are OH groups bonded with Fe, Mn and Mg ions while relatively stronger sites (m sites) are Fe-O, Mn-O and Mg-O ion pairs. Basing on cation charge/cation radius relation that characterized the basicity strength, one can obtain the following order of a decreasing of cation basicity: $Mg^{2+} > Mn^{2+} > Fe^{2+} > Fe^{3+}$. Note that this order is close to the order obtained above by the CO_2-TPD method for ferrite samples with the same cations.

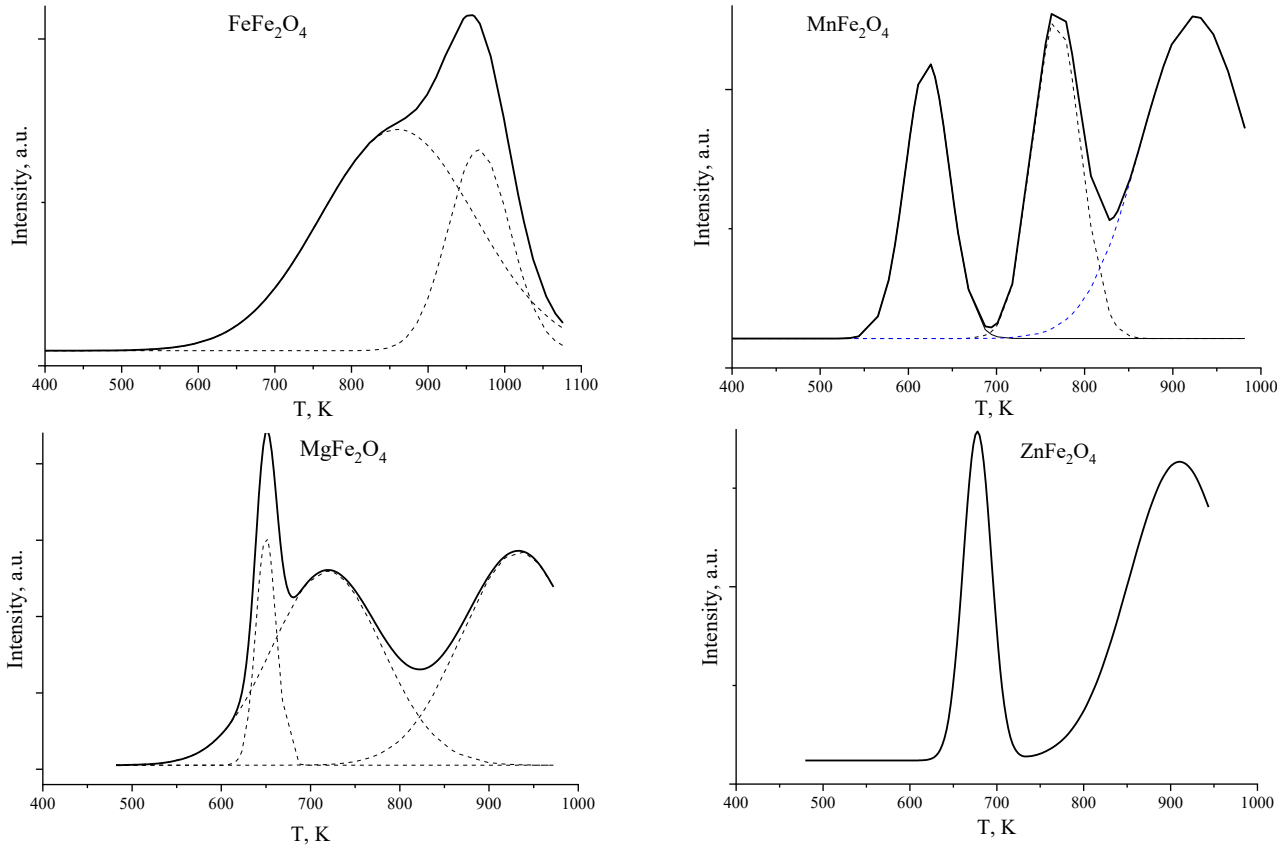

Fig.4. H_2-TPR profiles of $FeFe_2O_4$, $MnFe_2O_4$, $MgFe_2O_4$, and $ZnFe_2O_4$

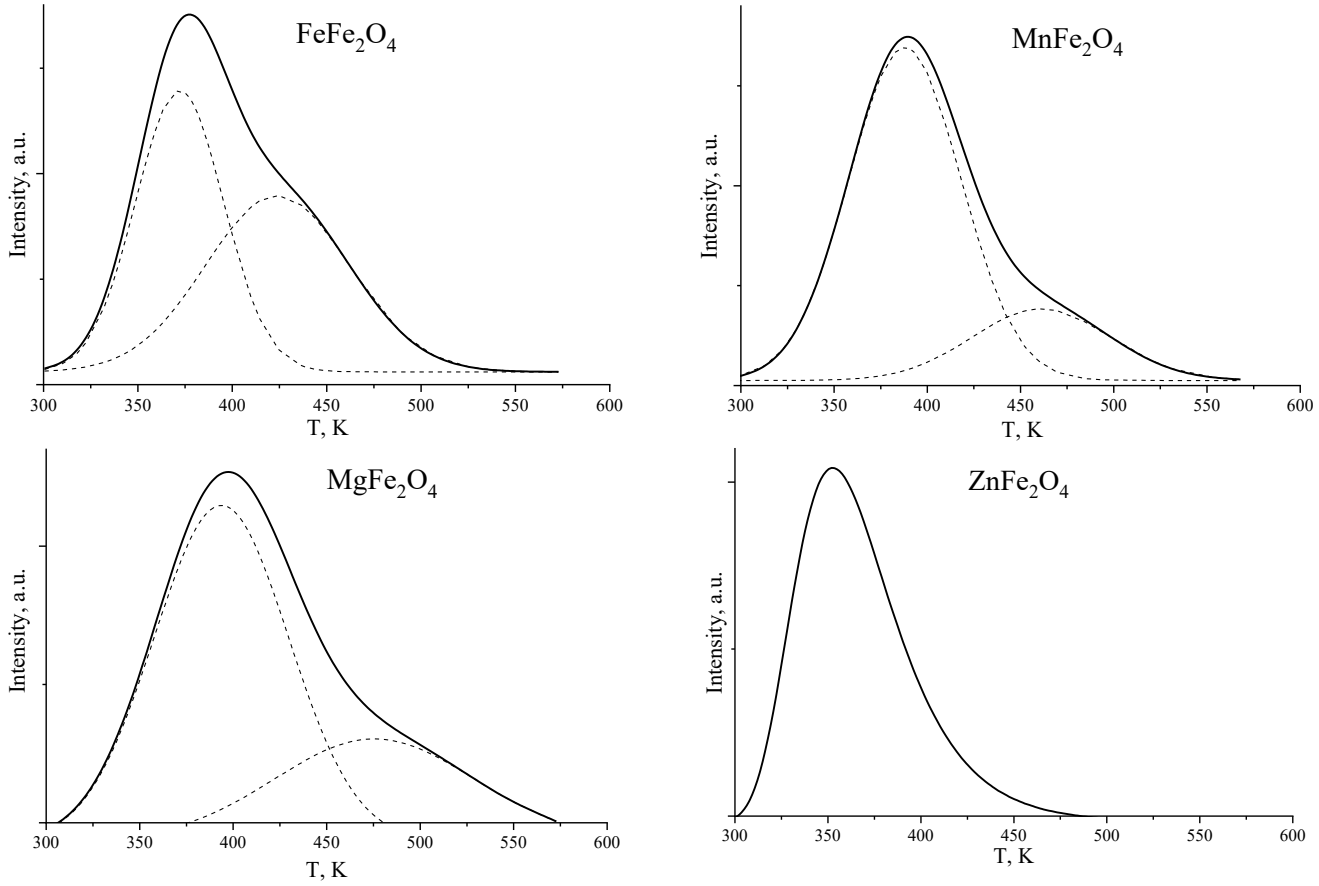

Fig.5. CO_2-TPD profiles of $FeFe_2O_4$, $MnFe_2O_4$, $MgFe_2O_4$ and $ZnFe_2O_4$

Table 2. **Temperatures of the CO_2 desorption peak maximum and amounts of chemisorbed CO_2 as determined by integration of the corresponding TPD profiles**

Ferrite	T_l, K	T_m, K	Relative amount of basic sites l %,	Relative amount of basic sites m %,	Total amount of desorbed CO_2,mmol·g^{-1},
$FeFe_2O_4$	372	423	49	51	0,21
$MnFe_2O_4$	388	461	79	21	0,18
$MgFe_2O_4$	394	476	69	31	0,32
$ZnFe_2O_4$	359	-	100	0	0,01

Ferrite catalytic properties in the ESR reaction

Table 3 presents the temperature dependencies of ethanol conversion, *X*, for the studied catalysts. The highest values of X were obtained for $FeFe_2O_4$ and $MnFe_2O_4$ in the temperature range of incomplete conversion.

The main reaction products were acetaldehyde, acetone, CO_2 and H_2; others were methane and C_2-C_4 hydrocarbons (HC) which formed in enough small amounts. It is important to note that CO was not detected in the reaction products.

The primary reaction in the ESR over ferrites can be the reaction of ethanol dehydrogenation to acetaldehyde [1-10]:

$C_2H_5OH = CH_3CHO + H_2$, (I)

Another common feature of the catalytic action of all investigated ferrites is a production of significant amounts of acetone at temperatures near 673 K. Acetone can be formed by reaction:

$2\ CH_3CHO+H_2O=CH_3COCH_3 +CO_2 +2\ H_2$. (II)

Also, ethanol can be directly converted to acetone, i.e. without intermediate formation of acetaldehyde in a gas phase:

$2\ CH_3CH_2OH + H_2O = CH_3COCH_3 + CO_2 + 4\ H_2$ (III)

Reaction (III) is especially probable for $FeFe_2O_4$; indeed, selectivity to acetone on this catalyst was near 60% already at 573 K, and it enhanced to 71.3% at 673 K (Table 3).

Summarily, acetaldehyde and acetone prevail over other reaction products. As seen from Fig.6, the experimental values of acetone and other reaction products for-$FeFe_2O_4$ are fairly close to their equilibrium values at 673 K. Here, thermodynamic calculations were made by procedure described in textbook [47] in supposition that only reactions (I) and (II) take place. Obtained results point out also that further transformation of acetone proceeds yet slow at 673 K, it becomes significant at more high temperatures. Therefore, the ferrite $FeFe_2O_4$ may serve as a promising catalyst for acetone producing from ethanol.

Table 3. **Temperature dependencies of ethanol conversion (X) and product selectivity for $MgFe_2O_4$, $MnFe_2O_4$, $FeFe_2O_4$, $ZnFe_2O_4$**

Ferrite	T, K	X, %	Selectivity, %				
			CH_3CHO	CH_3COCH_3	CO_2	C_1-C_4 HC	H_2
$MgFe_2O_4$	573	7,9	83,3	0	16,5	0,2	30,4
	623	23,7	21,6	55,9	21,3	1,2	31,1
	673	42,1	3,9	45,2	48,8	2,1	54,4
	723	85,9	0,9	43,1	52,8	3,2	57,6
	773	99,8	0,5	27,1	68,6	3,7	71,4
	823	99,9	0,3	14,1	81,2	4,4	82,4
$MnFe_2O_4$	623	36,8	0,8	62,7	33,1	3,4	40,2
	673	86,9	2,6	58,7	35,8	3,0	42,7
	723	98,3	3,8	40,0	47,6	8,6	51,8
	773	98,9	3,9	16,5	66,0	13,5	66,4
	823	98,9	1,1	4,7	85,0	9,1	84,3
$FeFe_2O_4$	573	9,6	18,8	60,1	20,2	0,8	30,0
	623	41,6	4,3	61,9	32,9	0,8	40,5
	673	88,7	2,9	71,3	24,3	1,4	32,7
	723	94,2	4,4	36,7	50,8	8,1	53,3
	773	97,8	1,4	18,1	60,7	19,8	56,7
	823	97,4	1,4	5,5	76,5	16,7	72,0
$ZnFe_2O_4$	573	5,3	99,7	0	0	0,3	16,6
	623	21,1	23,6	54,9	20,9	0,6	30,9
	673	28,9	21,7	56,2	21,4	0,6	31,2
	723	42,1	17,6	38,7	42,6	1,0	49,7
	773	46,0	17,3	22,4	58,2	2,1	63,4
	823	68,4	17,7	15,1	61,4	5,9	65,1

The surface metal cations $M^{\sigma+}$ in ferrites can be attributed to Lewis acid centers and oxygen anions $O^{\sigma-}$ to Brensted base centers. Probable mechanism of ethanol conversion to acetaldehyde may be as follows. Interaction of ethanol molecule with an acid-base pair $M^{\sigma+}$-$O^{\sigma-}$ leads to heterolytic O-H cleavage with formation of adsorbed ethoxy intermediate $CH_3CH_2O_{(a)}$ located on metal ion and proton located on surface oxygen ion. Next step is a β-elimination of hydride ion H^- from C-H bond in an ethoxy particle with transfer of H^- to the surface metal ion and desorption of acetaldehyde. Finally, a recombination of hydride ion and proton take place leading to the formation of gaseous molecular hydrogen. The main features of this mechanism were adopted from the work [48].

Adsorbed $CH_3CHO_{(a)}$ species can give rise to acetone formation via the aldol-type mechanism [49,50]:

$2CH_3\text{-}CHO_{(a)} + O_{(s)} \leftrightarrow CH_3\text{-}CH(OH)\text{-}CH_2\text{-}COO_{(a)} + H_{(a)}$ (IV)

$CH_3\text{-}CH(OH)\text{-}CH_2\text{-}COO_{(a)} + H_{(a)} \leftrightarrow CH_3\text{-}CO\text{-}CH_3 + CO_2 + H_2$ (V)

where $O_{(s)}$ is a lattice oxygen.

It is assumed that aldol condensation is catalysed by surface basic centers [49,50]. The presence of surface basic centers in the investigated ferrites was shown by the temperature programmed desorption of CO_2 (Fig.5). The removal of the surface oxygen in the step (V) leads to the formation of surface oxygen vacancies (with simultaneous decrease of the oxidation state of the nearest metal ions). Oxygen loss is compensated by the interaction of water with reduced surface centers as follows:

$H_2O + \square_{(s)} \leftrightarrow O_{(s)} + H_2$ (VI)

where $\square_{(s)}$ denotes a surface oxygen vacancy.

In more details, an oxygen vacancy may be presented as $[Fe^{2+}\square Fe^{2+}]_s$ species which is converted in reaction (VI) to $[Fe^{3+}O^{2-}Fe^{3+}]_s$. The reaction (VI) plays a very important role in the steam reforming of ethanol, first of all, because it gives up to 50% of hydrogen produced in the total ESR process.

The oxygen vacancies appear as a result of the reduction of the surface metal ions by gaseous and adsorbed organic compounds or their fragments like $CH_{3(a)}$, $CH_{2(a)}$, $CO_{(a)}$ as well as by hydrogen.

The overall reductive step in the ESR reaction can be expressed as

$CH_3CH_2OH + 3\,O_{(s)} \leftrightarrow 2\,CO_2 + 3\,H_2 + 3\,\square_{(s)}$ (VII)

At the temperatures higher 623-673 K, acetone selectivity decreases, while selectivity to CO_2 continues rising (Table 3). Obviously, it is due to the reaction of the steam reforming of acetone to CO_2 and H_2:

$CH_3COCH_3 + 5\,H_2O = 3\,CO_2 + 8\,H_2$ (VIII)

The data reported here show that the studied ferrites with spinel structure are active catalysts for the ESR reaction. Catalytic properties of spinels containing ions of transition metals depend on their redox properties as well as ion distribution between octahedral and tetrahedral sites in a spinel crystalline structure. Octahedral sites are exposed almost exclusively at the surface of the spinel oxides and the cations of these sites play the main role in the catalytic reaction [46, 51]. In particular, high activity of $MnFe_2O_4$ in the ESR reaction could be caused by the octahedral ions Fe^{3+} and Mn^{2+} that facilitate the red-ox transfer in M^{3+}/M^{2+} pairs. According to the TPR results, $MnFe_2O_4$ should more easy supply oxygen for oxidation of organic surface intermediates in comparison with $MgFe_2O_4$ and $ZnFe_2O_4$ thus selectivity to the mostly oxidized reaction product CO_2 and hydrogen is in whole higher for $MnFe_2O_4$.

Analysing the data for investigated ferrites (Table 3), one can deduce that an increase of temperature leads to a shift of the reaction product composition toward CO_2 and H_2, which is the target product of the ESR reaction. Fig.7 shows the temperature dependencies of hydrogen yield, Y_{H2}.

Maximum hydrogen yield is achieved at 823 K for $MnFe_2O_4$ (83,4 %). Note, that Y_{H2} value for $MnFe_2O_4$ prepared by decomposition of the heteronuclear complex $[MnFe_2O(CH_3COO)_6(H_2O)_3]\cdot 2H_2O$ was 94,6 % at 923 K [36].

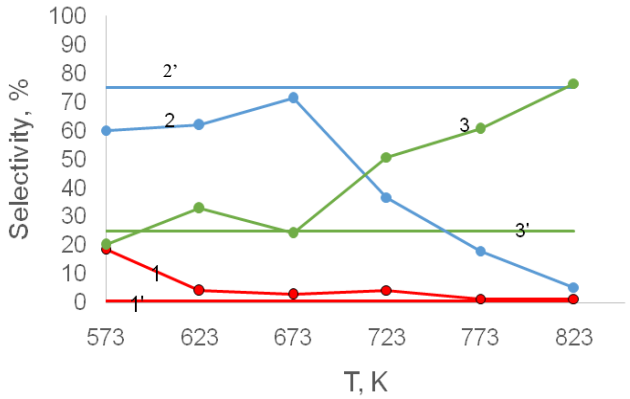

Fig. 6. Temperature dependencies of selectivity in the ESR process over $FeFe_2O_4$ at 2,7 mol.% C_2H_5OH, 50 mol.% H_2O, N_2 balance: experimental selectivity on acetaldehyde (1), acetone (2), CO_2 (3) and equilibrium selectivity on acetaldehyde (1'), acetone (2'), CO_2 (3').

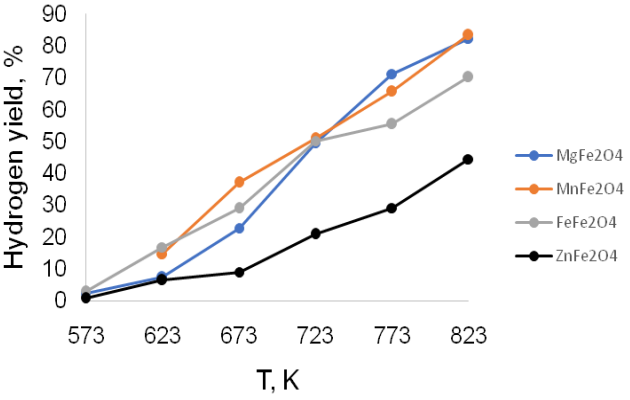

Fig.7. Temperature dependencies of hydrogen yield in the ESR process over $FeFe_2O_4$, $MnFe_2O_4$, $MgFe_2O_4$ and $ZnFe_2O_4$ at 2,7 mol.% C_2H_5OH, 50 mol.% H_2O, N_2 balance

Conclusions

The catalytic ethanol steam reforming was studied over the MFe_2O_4 (M = Fe, Mn, Mg, Zn) ferrites with the spinel structure prepared by co-precipitation method. The active phase of these catalysts is oxide phase because the catalysts remained in the unreduced state in the ESR conditions. Ethanol was firstly dehydrogenated to form acetaldehyde, which was then converted into acetone via condensation pathway. Besides, it is possible the direct way of ethanol conversion to acetone without intermediate formation of acetaldehyde in a gas phase. The formed acetone was further steam reformed to hydrogen and CO_2. It is important that products of the ESR reaction on the investigated ferrites do not contain CO.

In summary, the $FeFe_2O_4$, $MnFe_2O_4$ and $MgFe_2O_4$ ferrites could be considered as durable catalysts for hydrogen production via the ESR reaction. Moreover, the $FeFe_2O_4$ ferrite is efficient for the ethanol conversion to acetone, thus, it can be used, for example, as the catalyst of the first step in a two-step ESR reaction process or in other two-step processes which involve an intermediate formation of acetone.

References

1 Ghasemzadeh K., Jalilnejad E., Tilebon S.M.S. Hydrogen production technologies from ethanol. *Ethanol Science and Engineering*. Elsevier. 2018. 307-340.

2. Lazar M. D., Senila L., Dan M., Mihe M. Crude Bioethanol Reforming Process: The Advantage of a Biosource Exploitation. *Ethanol Science and Engineering*. Elsevier. 2018. 257-288.

3. Liu Z., Senanayake S.D., Rodriguez J.A. Catalysts for the Steam Reforming of Ethanol and Other Alcohols. *Ethanol Science and Engineering*. Elsevier. 2018. 133-158. 574 p.

4. Contreras J.L., Salmones J., Colin-Luna J.A., Nuno L., Quintana B., Cordova I., Zeifert B., Tapia C., Fuentes G.A. Catalysts for H_2 production using the ethanol steam reforming (a review). *Int. J. Hydrogen Energy*. 2014. 39. 18835-18853.

5. Pyatnitsky Y.I., Dolgykh L.Yu., Stolyarchuk I.L. Strizhak P.E. Production of hydrogen by steam reforming of ethanol. *Theor. Exp. Chem*. 2013. 49. 272-297.

6. Mattos L.V., Jacobs G., Davis B.H. Noronha F.B. Production of hydrogen from ethanol: review of reaction mechanism and catalyst deactivation. *Chem. Rev*. 2012. 112. 4094-4123.

7. Piscina P.R., Homs N. Use of biofuels to produce hydrogen (reformation processes). *Chem. Soc. Rev*. 2008. 37. 2459-67.

8. Ni M., Leung D.Y.C., Leung M.K.H. A review on reforming bioethanol for hydrogen production. *Int. J Hydrogen Energy*. 2007. 32. 3238-3247.

9. Vaidya P. D., Rodrigues A. E. Review. Insight into steam reforming of ethanol to produce hydrogen for fuel cells. *Chem. Eng. J*. 2006. 117. 39-49.

10. Haryanto A., Fernando S., Murali N., Adhikari S. Current status of hydrogen production techniques by steam reforming of ethanol: A review. *Energy & Fuels*. 2005. 19. 2098-2106.

11. Simson A., Farrauto R., Castaldi M. Steam reforming of ethanol/gasoline mixtures: Deactivation, regeneration and stable performance. *Appl. Catal. B*. 2011. 106. 295-303.

12. Bilal M., Jackson S.D. Ethanol steam reforming over Pt/Al_2O_3 and Rh/Al_2O_3 catalysts: The effect of impurities on selectivity and catalyst deactivation. *Appl. Catal. A*. 2017. 529. 98-107.

13. Palma V., Castaldoa F., Ciambellia P., Iaquaniellob G. CeO_2-supported Pt/Ni catalyst for the renewable and clean H_2 production via ethanol steam reforming. *Appl. Catal. B*. 2014. 145. 73-84.

14. Cifuentes B., Hernández M., Monsalve S., Cobo M. Hydrogen production by steam reforming of ethanol on a $RhPt/CeO_2/SiO_2$ catalyst: Synergistic effect of the Si:Ce ratio on the catalyst performance. *Appl. Catal. A*. 2016. 523. 283-293.

15. González-Gil R., Herrera C., Larrubia M.A., Mariño F., Laborde M., Alemany L.J. Hydrogen production by ethanol steam reforming over multimetallic $RhCeNi/Al_2O_3$ structured catalyst. Pilot-scale study. *Int. J. Hydrogen Energy*. 2016. 41.16786-16796.

16. Greluk M., Słowik G., Rotko M., Machocki A. Steam reforming and oxidative steam reforming of ethanol over $PtKCo/CeO_2$ catalyst. *Fuel*. 2016. 183. 518-530.

17. Auprêtre F., Descorme C., Duprez D. Bio-ethanol catalytic steam reforming over supported metal catalysts. *Catal. Comm*. 2002. 3. 263-267.

18. Liguras D.K., Kandarides D.I., Verykios X.E. Production of hydrogen for fuel cells by steam reforming of ethanol over supported noble metal catalysts. *Appl. Catal. B*. 2003. 43. 345-354.

19. Salge J.R., Deluga G.A., Schmidt L.D. Catalytic partial oxidation of ethanol over noble metal catalysts. *J. Catal*. 2005. 235. 69-78.

20. Cai W., Zhang B., Li Y., Xu Y., ShenW. Hydrogen production by oxidative steam reforming of ethanol over an Ir/CeO_2 catalyst. *Catal. Comm*. 2007. 8. 1588-1594.

21. Wang K., Dou B., Jiang B., Zhang Q., Li M., Chen H., Xu Y. Effect of support on hydrogen production from chemical looping steam reforming of ethanol over Ni-based oxygen carriers. *Int. J. Hydrogen Energy*. 2016. 41. 17334-17347.

22. Ramírez-Hernández G.Y., Viveros-García T., Fuentes-Ramírez R., Galindo-Esquivel I.R. Promoting behavior of yttrium over nickel supported on alumina-yttria catalysts in the ethanol steam reforming reaction. *Int. J. Hydrogen Energy*. 2016. 41. 9332-9343.

23. Biswas P., Kunzru D. Oxidative steam reforming of ethanol over Ni/CeO_2-ZrO_2 catalyst. *Chem. Eng. J*. 2008. 136. 41-49.

24. Frusteri F., Freni S., Chiodo V., Donato S., Bonura G., Cavallaro S. Steam and auto-thermal reforming of bio-ethanol over MgO and CeO_2 Ni supported catalysts. *Int. J. Hydrogen Energy* 2006. 31. 2193 - 2199.

25. Fatsikostas A.N., Kondarides D.I., Verykios X.E. Steam reforming of biomass-derived ethanol for the production of hydrogen for fuel cell applications. *J. Catal.* 2004. 225. 439-452.

26. Yu N., Zhang H., Davidson S.D., Sun J., Wang Y. Effect of ZnO facet on ethanol steam reforming over Co/ZnO. *Catal. Commun.* 2016. 73. 93-97.

27. Song H., Zhang L., Ozkan U.S. The effect of surface acidic and basic properties on the performance of cobalt-based catalysts for ethanol steam reforming. *Top. Catal.* 2012. 55. 1324-1331.

28. Song H., Ozkan U.S. Ethanol steam reforming over Co-based catalysts: Role of oxygen mobility. *J. Catal.* 2009. 261. 66-74.

29. Llorca J., Homs N., Sales J., Piscina1 P.R. Efficient production of hydrogen over supported cobalt catalysts from ethanol steam reforming. *J. Catal*. 2002. 209. 306-317.

30. Soykal I.I., Bayram B, Sohn H., Gawade P., Miller J. T., Ozkan U.S. Ethanol steam reforming over Co/CeO_2 catalysts: Investigation of the effect of ceria morphology. *Appl. Catal. A.* 2012. 449. 47-58.

31. Muroyama H., Nakase R., Matsui T., Eguchi K. Ethanol steam reforming over Ni-based spinel oxide. *Int. J. Hydrogen Energy*. 2010. 35. 1575-1581.

32. Barroso M.N., Gomez M.F., Arrua L.A., Abello M.C. Reactivity of aluminium spinels in the ethanol steam reforming reaction. *Catal. Lett*. 2006. 109. 13-19.

33. Li Z., Yi W., Qun H. Preparation and properties of K_2NiF_4-type perovskite oxides La_2NiO_4 catalysts for steam reforming of ethanol. *Trans. Nonferrous Met. Soc. China.* 2009. 19. 1444-1449.

34. Chen S.Q., Liu Y. $LaFe_yNi_{1-y}O_3$ supported nickel catalysts used for steam reforming of ethanol. *Intern. J. Hydrogen Energy*. 2009. 34. 4735-4746.

35. Ma F., Chu W., Huang L., Yu X., Wu Y. Steam reforming of ethanol over Zn-doped $LaCoO_3$ perovskite nanocatalysts. *Chin. J. Catal*. 2011. 32. 970-977.

36. Stolyarchuk I.L., Dolgikh L.Yu., Vasilenko I.V., Pyatnitsky Yu.I., Strizhak P.E. Catalysis of steam reforming of ethanol by nanosized manganese ferrite for hydrogen production. *Theor. Exp.Chem.* 2012. 48. 129-134.

37. Kim D.K., Mikhaylova M., Zhang Yu, Muhammed M. Protective Coating of superparamagnetic iron oxide nanoparticles. *Chem. Mater*. 2003. 15. 1617-1627.

38. Liu C.-P., Li M.-W., Cui Z. Huang J.-R., Tian Y.-L., Lin T., Mi W.-B. Comparative study of magnesium ferrite nanocrystallites prepared by sol–gel and coprecipitation methods. *J. Mater. Sci*. 2007. 42. 6133-6138.

39. Philip J., Gnanaprakash G., Panneerselvam G., Antony M. P., Jayakumar T., Raj B. Effect of thermal annealing under vacuum on the crystal structure, size, and magnetic properties of $ZnFe_2O_4$ nanoparticles. *J. Appl. Phys.* 2007. 102. 054305.

40. Dolgykh L., Stolyarchuk I., Deynega I., Strizhak P. The use of industrial dehydrogenation catalysts for hydrogen production from bioethanol. *Int. J. Hydrogen Energy*. 2006. 31. 1607-1610.

41. Giri J., Sriharsha T., Asthana S., Tumkur K., Rao G., Nigam A.K., Dhirendra B. Synthesis of capped nanosized $Mn_{1-x}Zn_xFe_2O_4$ ($0 \leqslant x \leqslant 0.8$) by microwave refluxing for bio-medical applications. *J. Magnet. Magnet. Mater*. 2005. 293. 55-61.

42. Rana S., Philip J., Raj B. Micelle based synthesis of cobalt ferrite nanoparticles and its characterization using Fourier transform infrared transmission spectrometry and thermogravimetry. *Mater. Chem. Phys*. 2010. 124. 264-69.

43. Rethwisch D.G., Dumesic J.A. Effect of metal-oxygen bond strength on properties of oxides. 1. Infrared spectroscopy of adsorbed carbon monoxide and carbon dioxide. *Langmuir*. 1986. 2. 73-79.

44. Jensen M.B., Pettersson L.G.M., Swang O., Olsbye U. CO_2 sorption on MgO and CaO surfaces: a comparative quantum chemical cluster study. *J. Phys. Chem. B.* 2005. 109 16774-16781.

45. Díez V.K., Apestegua C.R., Di Cosimo J.I. Aldol condensation of citral with acetone on MgO and alkali-promoted MgO catalysts. *J. Catal.* 2006. 240. 235-244.

46. Jacobs J.P., Maltha A., Reitjes J.G.H., Drimal J., Ponec V., Brongersma H.H., The surface of catalytically active spinels. *J. Catal*. 1994. 47. 294-300.

47. Pyatnytsky Y.I., Strizhak P. E. *Calculating Equilibrium and Simulating Kinetics of Heterogeneous Catalytic Reactions.* 2018, https://www.free-ebooks.net/ebook/Calculating-Equilibrium-and-Simulating-Kinetics-of-Heterogeneous-Catalytic-Reactions.

48. Schweitzer N.M., Hu B., Das U., Kim H., Greeley J., Curtiss L.A., Stair P.C., Miller J.T., Hock A.S. Propylene hydrogenation and propane dehydrogenation by a single-site Zn^{2+} on silica catalyst. *ACS Catal*. 2014. 4. 1091-1092.

49. Elliott D.J., Pennella F. The formation of ketones in the presence of carbon monoxide over $CuO/ZnO/Al_2O_3$. *J. Catal*. 1989. 119. 359-367.

50. Nishiguchi T., Matsumoto T., Kanai H., Utani K., Marsumura Y., Shen W., Imamura S. Catalytic steam reforming of ethanol to produce hydrogen and acetone. *Appl. Catal. A Gen*. 2005. 279. 73-77.

Надійшла до редакції 04.02.2020 р.

Ефективне одержання водню в паровому риформінгу етанолу на феритних каталізаторах

Л.Ю. Долгіх, І.Л. Столярчук, Л.А. Стара, І.В. Василенко, Ю.І. Пятницький, П.Є. Стрижак

Інститут фізичної хімії ім. Л.В. Писаржевського НАН України,
просп. Науки, 31, Київ 03028, Україна. E-mail: yupyat@gmail.com

Паровий риформінг етанолу на сьогодні є привабливим способом одержання водню як найбільш життєздатного носія енергії у майбутньому. Крім того, одержання водню з етанолу може бути екологічно сприятливим. Етанол може бути виготовлений з сільськогосподарських відходів, отже він є відновлювальним ресурсом. Його одержання шляхом ферментації біомаси є досить простим і дешевим способом. Крім експлуатаційних умов, вирішальну роль має використання каталізаторів для одержання водню шляхом риформінгу етанолу. Різні каталізатори були використані для парового риформінгу етанолу, у переважній більшості нанесені благородні метали, нікель і кобальт. Дана робота присвячена дослідженню парового риформінгу етанолу на феритах як нового типу оксидних каталізаторів цієї реакції. Феритні каталізатори, MFe_2O_4 (M = Mg, Mn, Fe, Zn), були приготовані методом співосадження; для характеристики каталізаторів використовували методи рентгенофазового аналізу, дифракції електронів, БЕТ, температурно-програмованої десорбції CO_2, термічної гравіметрії. Каталітичні експерименти здійснювали за атмосферного тиску у діапазоні температур 573-823 K. Основними продуктами реакції були ацетальдегід, ацетон, CO_2 і H_2. Важливо відзначити, що CO, який є небажаною домішкою до водню, не міститься в продуктах реакції. При відносно низьких температурах висока селективність за ацетоном (71,3 %), яка дуже близька до її теоретичної величини (75 %), спостерігалася для $FeFe_2O_4$. Таким чином, ферит $FeFe_2O_4$ може бути ефективним каталізатором прямого перетворення етанолу у ацетон. За високих температур селективність за ацетоном зменшується внаслідок конверсії ацетону у CO_2 і цільовий продукт H_2. Селективність за воднем збільшується при підвищенні температури до 823 K для усіх вивчених феритів. Максимум виходу водню (83,4 %) було досягнуто на $MnFe_2O_4$, тому він є перспективним об'єктом для подальших досліджень.

Ключові слова: етанол, паровий риформінг, феритні каталізатори, водень